PNAS
www.pnas.org

# Supplementary Information for

## Identification of a new subset of lymph node stromal cells involved in regulating plasma cell homeostasis

Hsin-Ying Huang, Ana Rivas-Caicedo, François Renevey, Hélène Cannelle, Elisa Peranzoni, Leonardo Scarpellino, Debbie L. Hardie, Arnaud Pommier, Karin Schaeuble, Stéphanie Favre, Tobias K. Vogt, Fernando Arenzana-Seisdedos, Pascal Schneider, Christopher D. Buckley, Emmanuel Donnadieu and Sanjiv A. Luther

Correspondance to: Sanjiv A. Luther
Email: sluther@unil.ch

**This PDF file includes:**

Supplementary text
Figs. S1 to S7
Tables S1 to S2
Captions for movies S1 to S7
References for SI citations

**Other supplementary materials for this manuscript include the following:**

Movies S1 to S7



www.pnas.org/cgi/doi/10.1073/pnas.1712628115

# Supplementary Information Text

## Supplemental Experimental Procedures.

**Mouse manipulations.** Mice were 8-12 weeks of age. For BrdU administration, 1mg BrdU was injected i.p. at the time of immunization and then continuously provided in drinking water (0.8 mg/mL).

**Histological visualization of conduits and labeling of thick sections.** For the detection of functional conduits, 100 µg Texas Red-labeled 10 kDa dextran (Molecular Probes) was injected subcutaneously, fixed in 1% PFA, saturated in 30% sucrose, embedded in Tissue-Tek OCT (Sakura) and frozen in an ethanol dry ice bath. For immunofluorescence staining of thick vibratome sections (320 µm), activated pLN (SRBC or OVA/Mont) were fixed for 2h at RT with PLP buffer (0.05 M phosphate buffer containing 0.1 M L-lysine [pH 7.4], 2 mg/ml $NaIO_4$, and 10 mg/ml paraformaldehyde). Antibody incubations and wash steps lasted several hours to allow penetration of thick sections. Confocal imaging allowed to gather 3D image stacks.

**Microscopy and image analysis.** SHG imaging of fibrillar collagen within LN of pCol-GFP mice was performed with a DM500B upright microscope equipped with a SP5 confocal head (Leica). Excitation was provided by a Chameleon Ultra Ti:Sapphire laser (Coherent) tuned at 800 nm. Emitted fluorescence was split with a 560 nm dichroic mirror and passed through a 465/30 (SHG) and 525/50 (GFP) bandpass filters to non-descanned detectors. Images were acquired with a 25x water immersion objective (Olympus, 20x/0.95 NA). During acquisition, image fields were acquired across the entire tissue section and stitched together to form a single high-resolution, large field-of-view image.

**Imaging of plasma cell motility within live LN slices.** pLN slice preparation was as previous described (1). In brief, activated pLNs were initially embedded in 4% low-gelling-temperature agarose (type VII-A; Sigma-Aldrich) prepared in PBS. 320 µm slices were cut with a vibratome (VT 1000S; Leica) in a bath of ice-cold PBS. Slices were submerged in RPMI 1640 plus 10% FCS at 4°C for a few minutes and were transferred to 0.4-µm organotypic culture inserts (Millicell; Millipore) in 35-mm Petri dishes containing 1 ml RPMI 1640 plus 10% FCS in an incubator at 37°C/6% $CO_2$. To image the distribution of PB/PC plated on top of vibratome sections of activated LN from pCol-GFP mice, PB ($CD138^+B220^{high}$) and PC ($CD138^+B220^{low}$) were purified from activated pLN (OVA/Mont d7) by a FACSAria sorter (90% purity) and then stained with either 0.5 µg/ml Hoechst (Invitrogen) or 0.5 µM 5-chloromethylfluorescein diacetate (CMFDA; Invitrogen) for 5 min at 37°C in HBSS, and then washed in RPMI 1640 plus 10% FCS and resuspended in this medium. In some experiments, PB/PC cells were pretreated for 2 hours with 100 ng/ml PTX (Calbiochem) at 37°C. A total of 1 x $10^5$ lymphocytes in 10-20 µl was added onto the cut surface of each slice. Slices were incubated for 1 h at 37°C, 6% $CO_2$, gently washed to remove the residual cells that have not entered the tissue, and kept at 37°C, 6% $CO_2$ before

imaging. PB/PC were imaged with a SP5 confocal (Leica) equipped with a chamber kept at 37°C. For dynamic imaging, slices were secured with a stainless steel washer and perfused with a solution of RPMI without phenol red bubbled with 95% $O_2$ and 5% $CO_2$ at a rate of 1 ml/min. Images were acquired with a 25x water immersion objective (Olympus, 20x/0.95 NA). For four-dimensional analysis of cell migration, stacks of 8 sections (z step = 10 µm) were acquired every 20 s for 20 min, at depths up to 60 µm. Imaging was usually done at least 10 µm below the cut surface of the slice. Videos were made by compressing the z information into a single plane with the best focus function of Metamorph. Cellular motility parameters, cell numbers as well as duration of cell-cell contact were calculated using Imaris software 7.1 (Bitplane AG). Only cells localized at least 10 µm below the surface of the slice were included in the analysis.

# Supplementary Figures and Tables

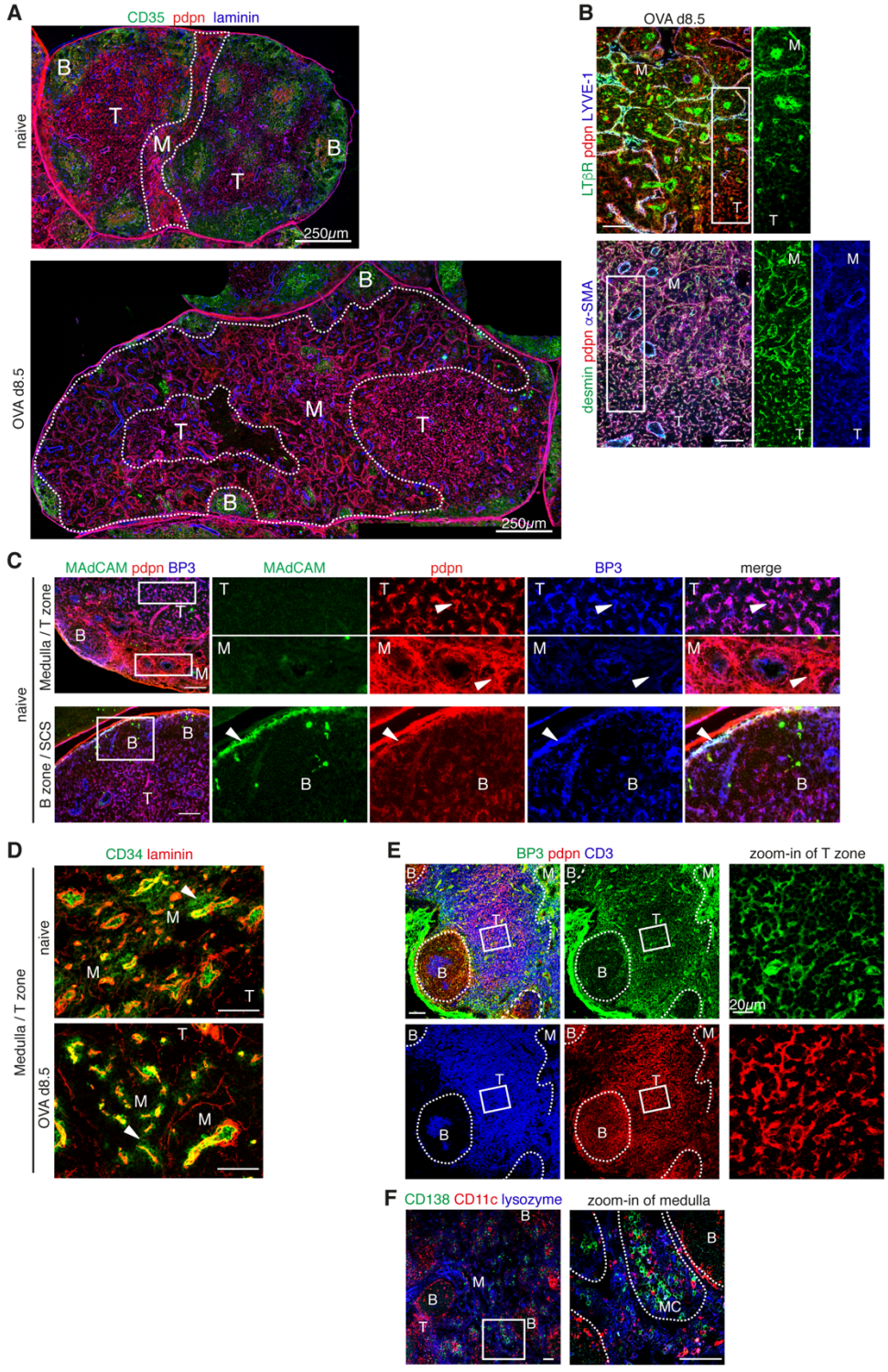


**Fig. S1. Histological characterization of FRC subsets in naive and activated lymph nodes (related to Fig. 1).** Immunofluorescence microscopy of cryostat sections from pLN of naive or

OVA/Mont-immunized mice (including OT-I/II cell transfer) (**A-D**) and from human LN (**E-F**). (**A**) Sections adjacent to those shown in Figure 1A, stained with the indicated antibodies, showing the extensive growth of the medullary cords upon LN activation. (**B**) Sections from activated pLN were stained with the indicated antibodies. The boxed areas are represented on the right side at higher magnification and with single colors. (**C**) Sections from naive pLN were stained for pdpn, MAdCAM and BP3. The boxed areas are represented on the right side at higher magnification and with single or merged colors. (**D**) Sections labeled for CD34 and laminin to indicate that only a subset of MedRC expresses CD34 with a preferential perivascular localization. (**E-F**) Sections of human pLN were stained with the indicated antibodies. Boxed areas are shown at higher resolution. B, B cell follicle; T, T cell zone; M, medulla; SCS, subcapsular sinus; scale bar, 100µm (except if indicated otherwise). Results are representative for at least three independent mice or human samples.

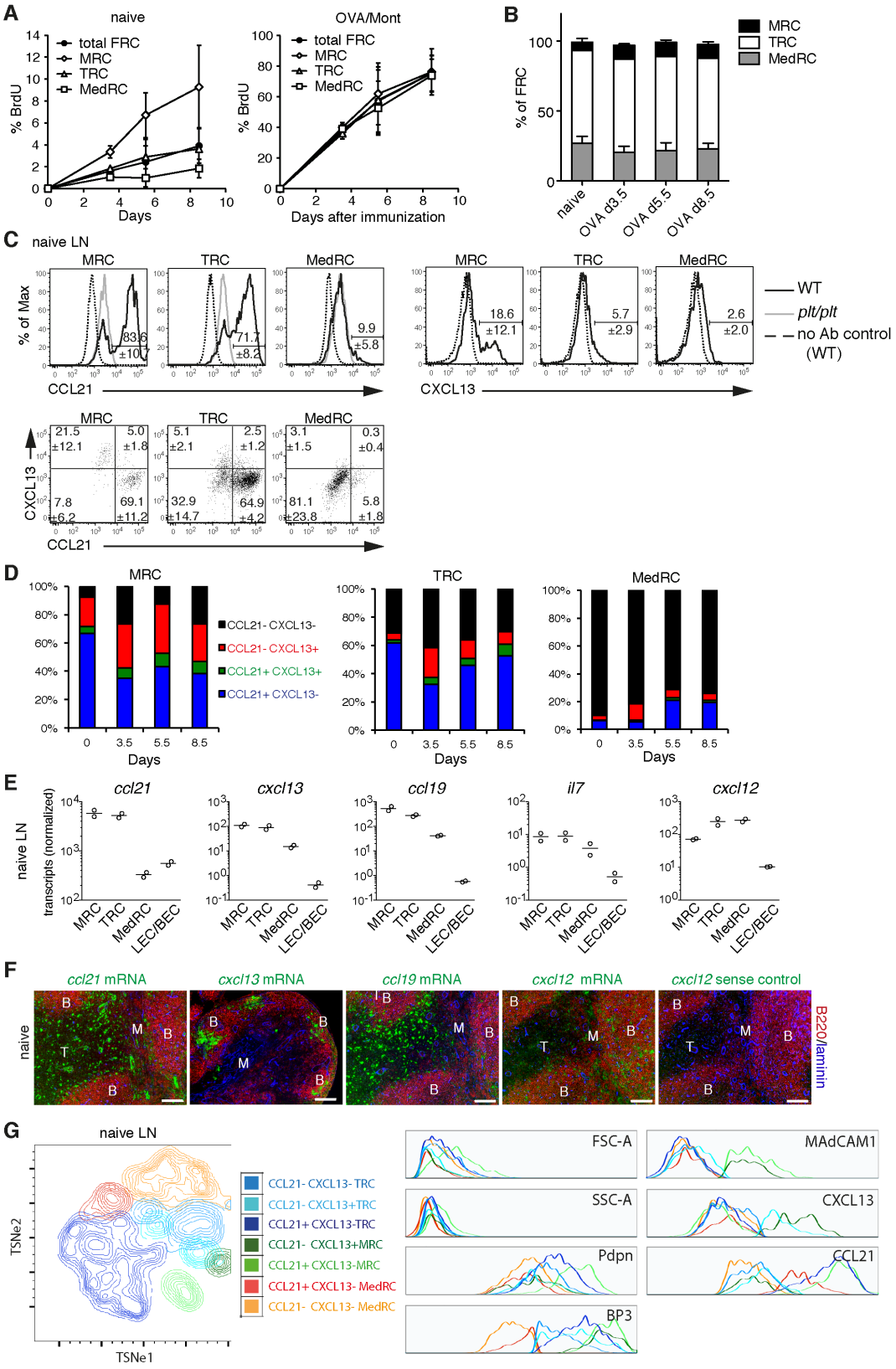


**Fig. S2. Flow cytometric and transcriptional characterization of FRC subsets in naive and activated lymph nodes (related to Fig. 2).** (**A-D**) Flow cytometric analysis of FRC (CD45$^-$31$^-$35$^-$

) of naive or OVA/Mont-immunized mice (including OT-I/II cell transfer) at the indicated time points and separated into the three FRC subpopulations based on MAdCAM and BP3 expression. Shown are the % of $BrdU^+$ cells among total FRC or FRC subsets (**A**), and the relative proportion of FRC subsets (**B**) among total FRC in homeostasis and during immune response. (**C**) Representative histograms and dot plots displaying the frequency of CCL21- and CXCL13-expressing cells among the three FRC subsets (black line) in naive pLN, as well as analysis of no primary antibody negative controls on total FRC (dashed line). For CCL21 staining, cells from *plt/plt* mice (deficient in *CCL19* and *CCL21ser*) were used as an additional negative control (grey line). (**D**) Frequency of cells expressing intracellular CCL21- and CXCL13 among the three FRC subsets found in naïve and activated pLN (*n*=12; 6; 6; 3). (**E**) The level of the indicated chemokine and cytokine transcripts was assessed by qRT-PCR in the three FRC subsets and $CD31^+$ cells (LEC/BEC) sorted from pLN of naive mice. The data present duplicate ± SEM. (**F**) *In situ* hybridization analysis of naive pLN for the indicated chemokine and cytokine transcripts (green) along with antibody staining for B220 and laminin. As negative control the sense probe for CXCL12 is shown. B, B cell follicle; T, T cell zone; M, medulla; scale bar, 100µm. Results in A-D and F are representative for at least three independent mice. (**G**) Multi-parameter flow cytometry based clustering of FRC (CD45-31-pdpn+) subsets from naïve pLN using the TSNe algorithms (Flowjo) to display 7 parameters (FCS, SSC, Pdpn, BP3, MAdCAM-1, CXCL13 and CCL21; shown on the right) in a 2D representation (left panel; contour plot of same data as shown in Figure 2H).

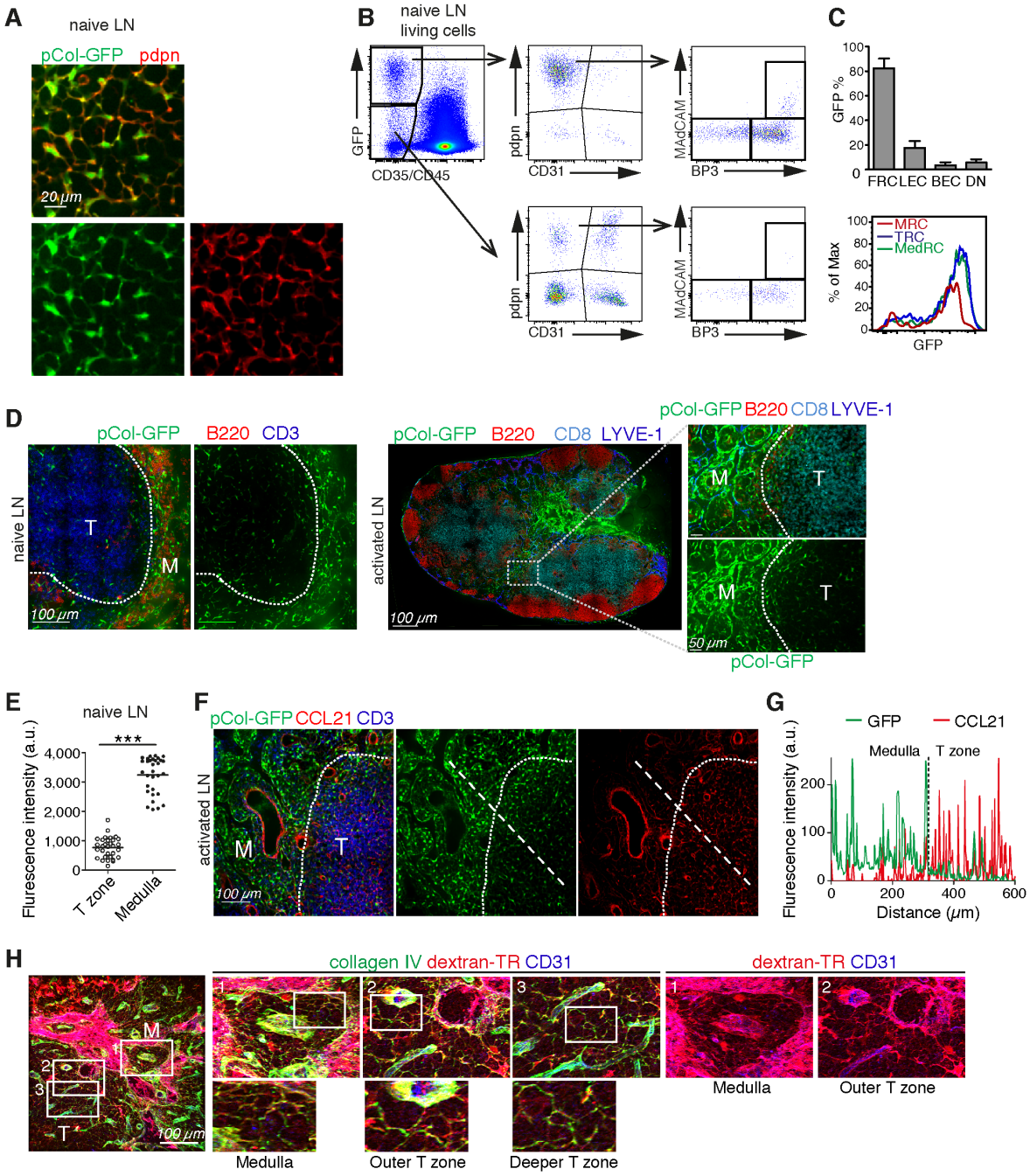


**Fig. S3. Flow cytometric and histological characterization of matrix production and arrangement by MedRC in activated lymph nodes (related to Fig. 3).** (**A**) Immunofluorescence staining of naive pLN from pCol-GFP mice for GFP and pdpn. (**B**) Representative flow cytometric analysis of LN cell suspensions from naive pCol-GFP mice with arrows showing the sequential gating strategy used to study various stromal cells. (**C**) Top: Percentage of cells expressing GFP in the following $CD45^{-}CD35^{-}$ LN stromal cell populations: $pdpn^{+}CD31^{-}$ FRC, $pdpn^{+}CD31^{+}$ LEC, $pdpn^{-}CD31^{+}$ BEC and $pdpn^{-}CD31^{-}$ DN cells. Bottom: Histogram showing the GFP expression profile for the three FRC subsets. (**D**) Confocal

microscopy of naive or activated (SRBC, d7) pLN from pCol-GFP mice. Vibratome sections were stained with the indicated antibodies. Dashed lines highlight the border between the T zone and the medulla. The boxed area is highlighted at higher magnification on the right side. (**E**) Graph showing the GFP fluorescence intensity of fibroblasts found in the T cell zone and MC of pLN from naive pCol-GFP mice. (**F**) Immunofluorescence staining of SRBC-activated pLN of pCol-GFP mice for GFP, CCL21 and CD3. (**G**) Histogram showing the fluorescence intensity of GFP and CCL21 along the dashed line shown in (**F**). (**H**) Vibratome section of pLN (OVA d5.5) 10 min after s.c. injection of Texas Red (TR)-dextran (10 kD) and stained for collagen IV and CD31. The boxed areas are represented on the right side at higher magnification with a further magnification shown below. Area 1 represents a MC, area 2 an outer T zone and area 3 a more central T zone. T, T cell zone; M, medulla. Results are representative for at least 2-3 mice and two independent experiments.

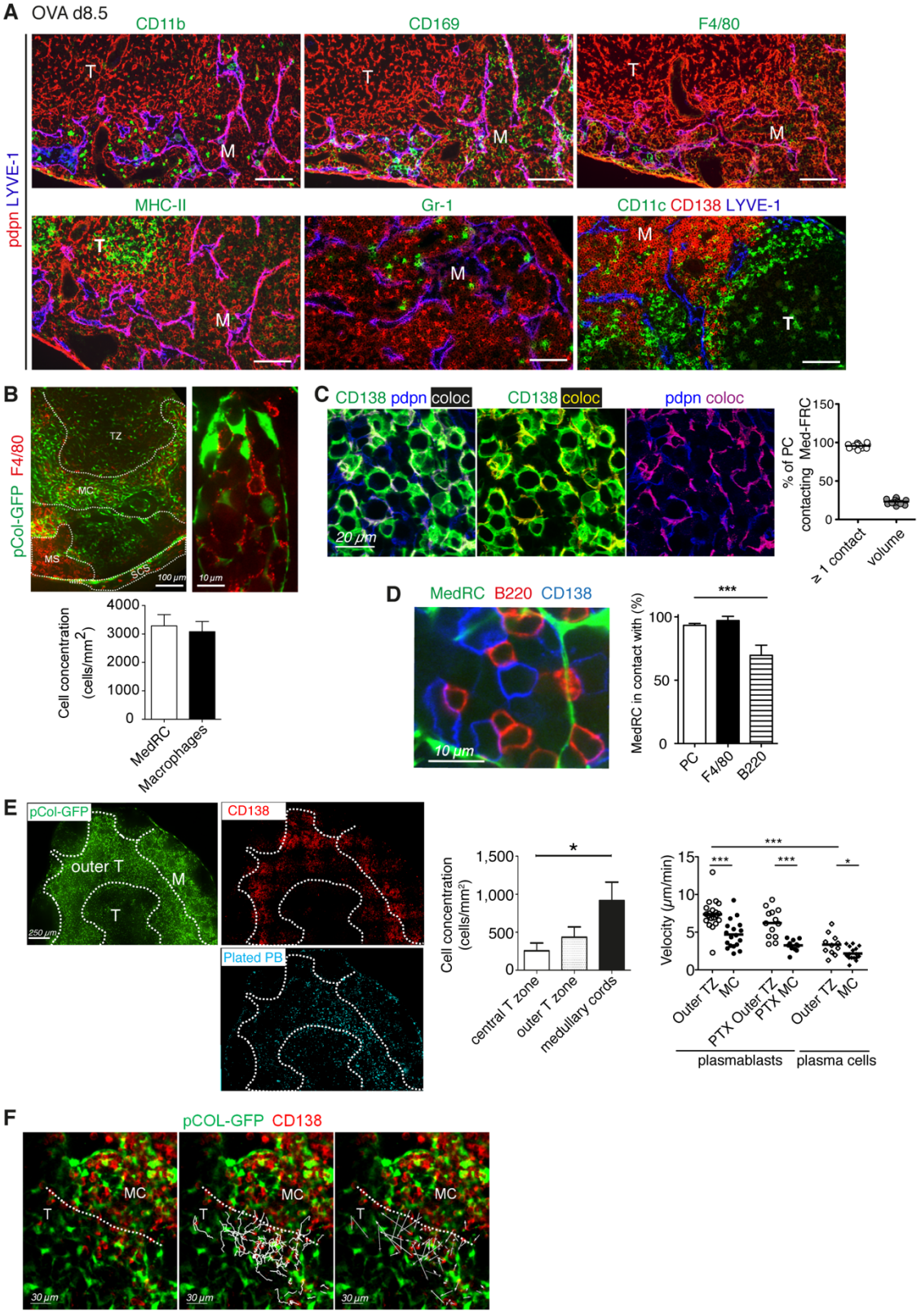


**Fig. S4. Histological evidence of niche forming cells and PC migration into the medullary cords (related to Fig. 4).** (**A**) Immunofluorescence staining of the T zone and MC of activated

pLN from OVA/Mont immunized mice (d8.5) for pdpn and LYVE1 along with various myeloid cell markers (either CD11b, CD169, F4/80, MHC-II or Gr-1). The bottom image shows $CD11c^+$ cells along with CD138 and LYVE1. *n*=3. (**B**) Confocal images of vibratome sections of pLN (SRBC d7) from pCol-GFP mice stained with the F4/80 antibody (red). Bottom: concentration of $F4/80^+$ cells and MedRC in medullary cords. *n*= 6 pLN slices. (**C**) 3D reconstruction (3µm in z-axis) of confocal images of vibratome sections from pLN (OVA/Mont d5.5) stained with the indicated antibodies. White areas represent contact zones between PC and FRC. Right: The % volume of PB/PC surface contacting MedRC, or the % of PB/PC showing at least one direct contact with a MedRC. *n*= 7 pLN slices. See also Movie S2. (**D**) A confocal image of an activated pLN from a pCol-GFP mouse stained with the indicated antibodies. Frequency of MedRC in contact with PC, F4/80+ and B220+ cells (*n*= 7 areas in 2 pLN slices). (**E**) Localization and migration of fluorescently labeled $CD138^+B220^{int}$ PB plated on top of live vibratome sections relative to $GFP^+$ FRC in the T zone (TZ), outer TZ and MC from activated pLN of pCol-GFP mice. Left: representative examples of labelled tissue sections. Middle: Graph showing the concentration of PB infiltrated into these three zones. Right: Graph showing the track velocity of $CD138^+$ $B220^{int}$ PB pretreated or not with pertussis-toxin (PTX), or $CD138^+$ $B220^{low}$ PC, 1 hour after having been plated on top of the sections (see materials and methods for details). Track velocities were measured in the outer TZ and MC. T, T cell zone; M, medulla; scale bar, 100µm. Values are from 3 experiments in which cells were tracked from 6 pLN slices. (**F**) Motility pattern of PC/PB (red) in a representative LN slice from an immunized pCol-GFP mouse. Also shown are tracks (middle) and trajectory vectors (right) during a 20-minute recording. See also Video S3.

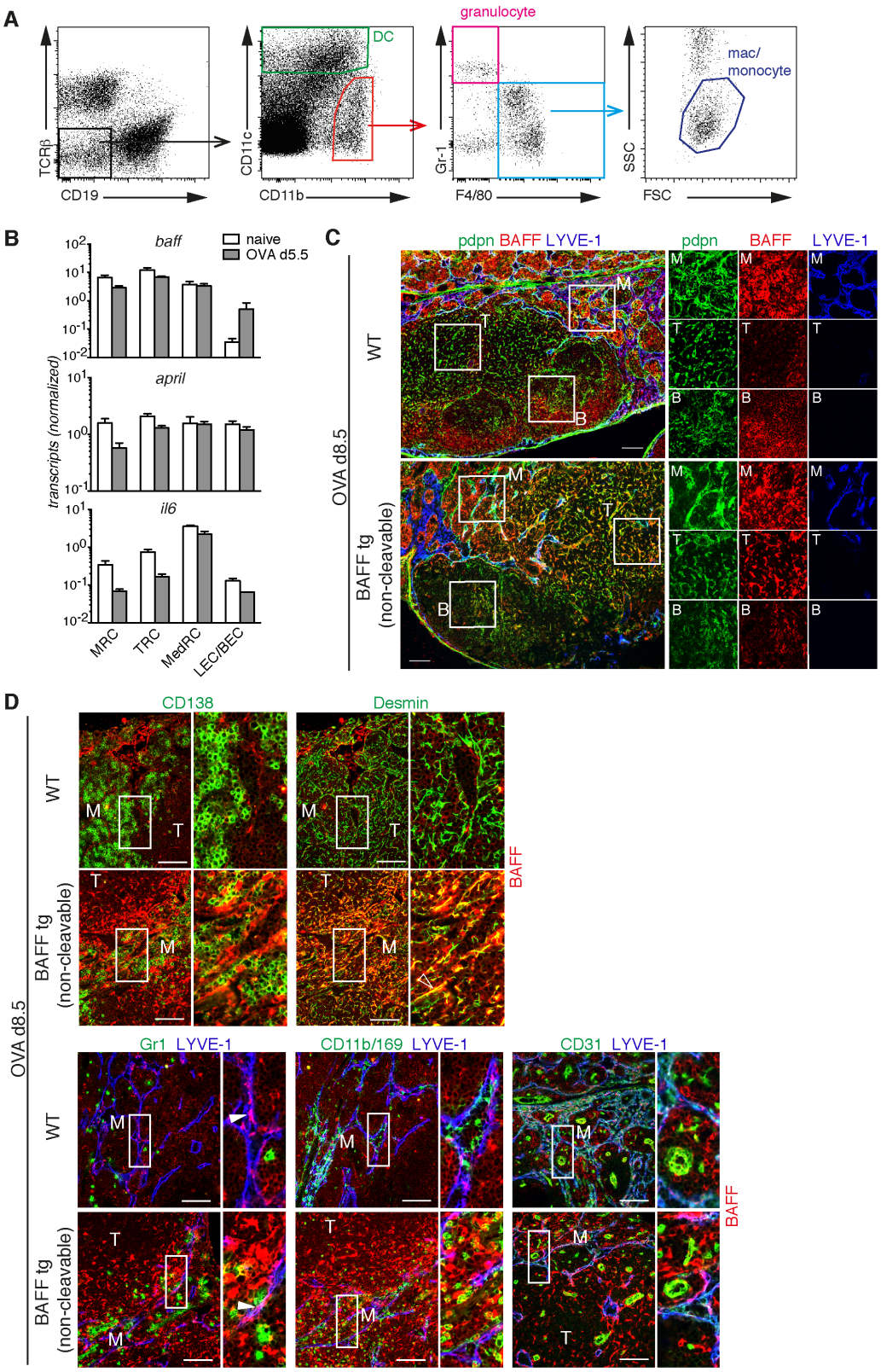


**Fig. S5. Expression of plasma cell survival factors by medullary FRC (related to Fig. 5).** Mice were immunized or not with OVA/Mont (including OT-I/II cell transfer) and draining pLN

analyzed. (**A**) Flow cytometric gating strategy of macrophages/monocytes, DC and granulocytes with gates and arrows showing the sequential gating. (**B**) The level of *baff*, *april* and *il-6* transcripts was assessed in the four stromal cell subsets sorted from naive pLN. To facilitate the comparison with the levels observed in these subsets found in d5.5-activated pLN the data from Figure 5A are shown again in grey bars. Error bars present SEM (naïve *n*=2, OVA *n*=4). (**C**) Immunofluorescence staining of d8.5-activated pLN from WT and uncleavable BAFF transgenic mice for BAFF expression (red) in $Pdpn^{+}LYVE1^{-}$FRC and $Pdpn^{+}LYVE1^{+}$ lymphatic vessels in medulla. The areas shown as white square are represented at higher magnifications with single colors on the right side. (**D**) Additional immunofluorescence stainings on d8.5-activated pLN from WT and uncleavable BAFF transgenic mice for BAFF, CD138, Gr-1, CD11b/CD169 (combined), CD31, desmin and LYVE1.

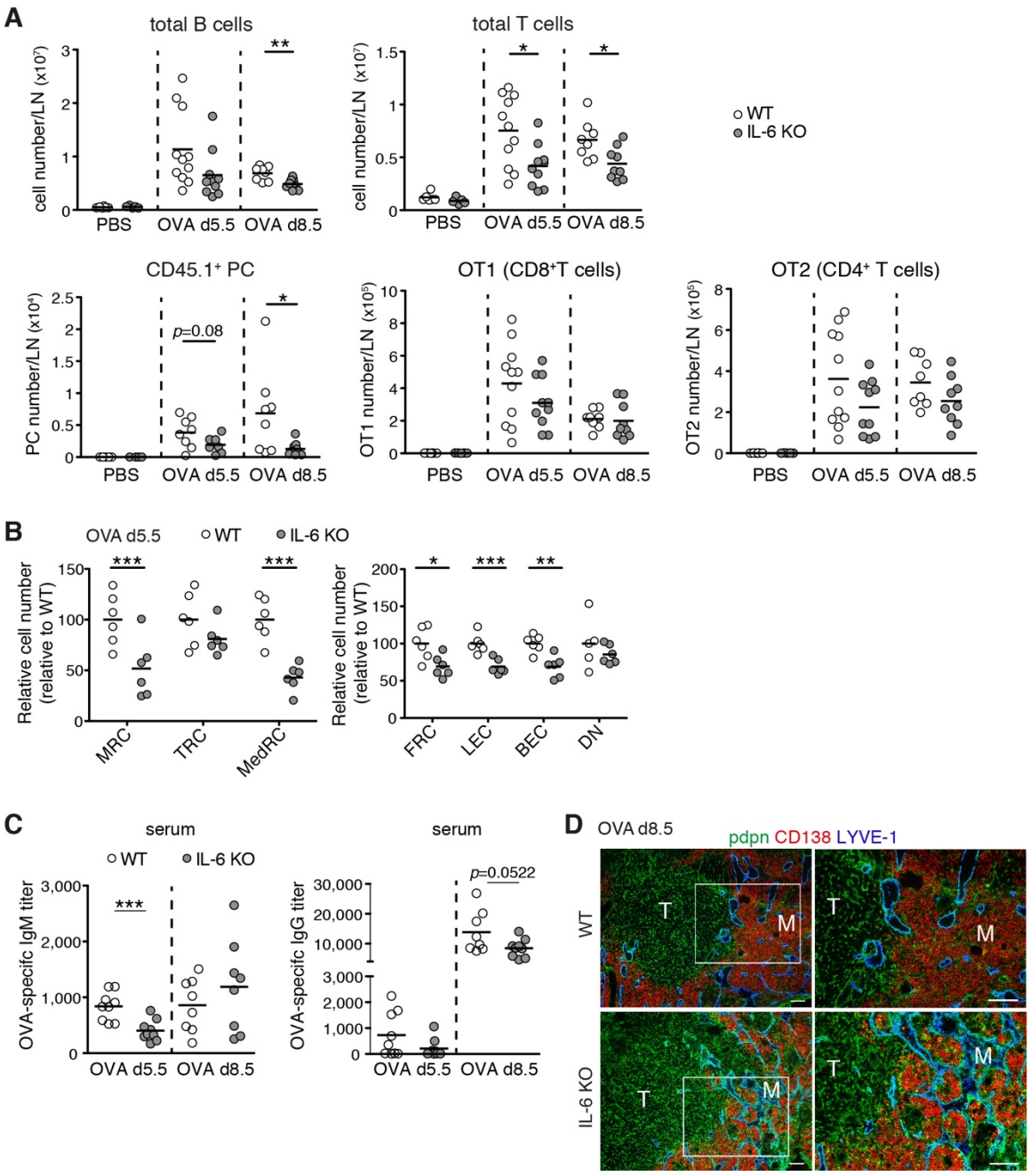


**Fig. S6. Evidence for a role of IL-6 in promoting PC survival in vivo (related to Fig. 6).** pLN of WT or IL-6 KO mice injected with PBS or OVA/Mont (including OT-I/II cell transfer) were analyzed for stromal and hematopoietic cells as well as their responses. (**A**) Number of total B and T cells (upper panel), PB/PC (bottom left panel), OT-I (bottom middle panel) or OT-II (bottom right panel) T cells. CD45.1$^{+}$ OT T cells were from wt mice and therefore capable of producing IL-6. (**B**) The relative cell number of FRC subsets (left panel) and other stromal cells (right panel). (**C**) Titers of OVA-specific IgM and IgG in serum. (**D**) pLN sections stained with the indicated antibodies. The white square is represented at a higher magnification on the right side. *n*=3. T zones (T), medulla (M); scale bar, 100μm.

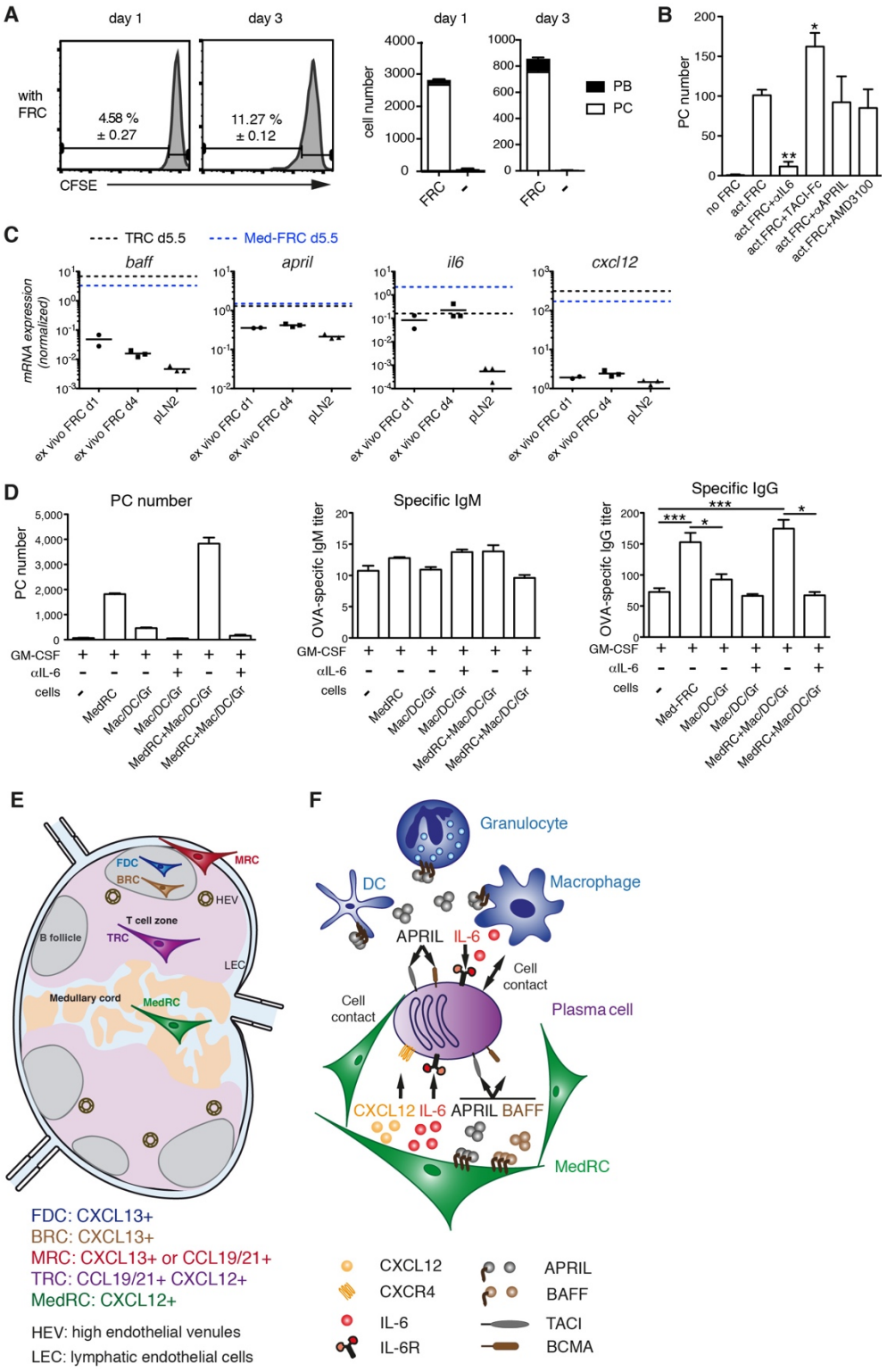


**Fig. S7. In vitro evidence for medullary niche cells promoting PC survival (related to Fig. 7 and the discussion).** Mice were immunized with OVA/Mont (including OT-I/II transfer) and

draining pLN used on d5-8 for isolation of either PB/PC or potential support cells, such as stromal or myeloid cells. (**A**) Histograms (left side) and bar graph (right side) showing the percentage or numbers, respectively, of dividing plasmablasts versus non-dividing plasma cells as measured by CSFE dilution on day 1 and 3 of coculture with enriched FRC or without FRC. Similar data were obtained on day 1 by EDU incorporation (6 +/- 4 %) in presence of FRC (not shown). (**B**) Number of surviving PC after coculture with enriched FRC from activated pLN in presence of inhibitors for IL-6 (αIL-6), APRIL (αAPRIL), APRIL and BAFF (TACI-Fc) or CXCL12 (CXCR4 inhibitor). *n*=2-3. (**C**) The level of *baff*, *april*, *cxcl12* and *il6* transcripts was measured by qRT-PCR from enriched ex vivo FRC of d5.5-activated pLN or from the FRC line (pLN2) after 1 or 4 days of culture. Average transcript levels of TRC (black dashed line) and MedRC (blue dashed line) sorted from LN of OVA/Mont-immunized mice (d5.5) are shown as comparison with data reproduced from Figure 2E and Figure S5B. (**D**) MACS-purified PB/PC were cocultured for 3 days with various FACS-sorted cell populations (as in Figure 7) in the indicated conditions (+/- rIL-6, +/- GM-CSF) followed by the analysis of surviving PCs by flow cytometry (B220 $^{low/-}$CD138$^{+}$CD44$^{+}$IgM$^{-}$FSC$^{hi}$SSC$^{hi}$) or of IgM or IgG antibody titers in the culture supernatant by ELISA. *n*=2-4. Error bars present SEM.*$p$<0.05, **$p$<0.01, *** $p$<0.001. (**E**) Model showing the four major FRC subsets in LN. Medullary FRC (MedRC) are anatomically, phenotypically and functionally distinct from FDC in B zones, FRC of T zones (TRC), as well as from MRC found below the subcapsular sinus. Localized in medullary cords of activated lymph nodes, MedRC lack expression of the classical B and T zone chemokines, CXCL13 and CCL19/21, besides lacking the naïve T cell survival factor IL-7, but have specialized roles in plasma cell (PC) biology, as detailed in the adjacent model. (**F**) Proposed model for MedRC function in activated lymph nodes. MedRC provide physical guidance for PC migration, including a 3-dimensional meshwork forming niche-like structures, in which PC can access survival factors produced in large amounts by MedRC, including CXCL12, IL-6 and BAFF. CXCL12 may play additional roles in attracting PC within MC and/or retaining them there. Similar to the evidence for mixed PC niches in the bone marrow, the lymph node equivalent is also composed of fibroblasts and myeloid cells, with these cells forming together niches that positively and possibly negatively regulate PC survival.

**Table S1. Antibodies used in flow cytometry (FACS) and immunofluorescence (IF) staining of mouse and human tissues.**

| Primary antibodies for mouse tissues | Clone or source | Supplier | Note |
|---|---|---|---|
| αSMA | 1A4 | Sigma | IF |
| BAFF | goat | R&D Systems | IF |
| B220 | RA3-6B2 | In house | FACS, IF |
| BP3/CD157 | BP-3 | Biolegend | FACS, IF |
| CCL21 | goat | R&D Systems | FACS, IF |
| CCL21 | rabbit | Peprotech | FACS, IF |
| CXCL12/SDF1pan (mouse/human) | K15C | In house | IF |
| CXCL13 | goat | R&D Systems | FACS, IF |
| CD11b | M1/70 | In house, Biolegend | FACS IF |
| CD11c | HL3 | BD Biosciences | IF |
| CD11c | N418 | In house, eBioscience | FACS, IF |
| CD138 | 281-2 | BD Biosciences | FACS, IF |
| CD169 | 3D6.112 | AbD Serotec | IF |
| CD19 | 6D5 | In house | FACS |
| CD21/35 | 7E9 | Biolegend | FACS |
| CD3 | 145-2C11 | In house, eBioscience | IF |
| CD31 | GC-51 | In house | IF |
| CD31 | 390 | Biolegend | FACS |
| CD34 | RAM34 | eBioscience | IF |
| CD4 | RM4-5 | eBioscience | FACS |
| CD44-FITC | IM7 | In house | FACS |
| CD45.1 | A20.1 | In house, Biolegend | FACS |
| CD45.2 | 104 | eBioscience | FACS |
| CD45pan | 30-F11 | Biolegend, eBioscience | FACS |
| CD8α | 53-6.7 | In house, Biolegend | FACS, IF |
| Collagen I or IV (mouse/human) | goat | Southern Biotech | IF |
| Desmin | rabbit | Progen | IF |
| F4/80 | F4/80 | In house | IF |
| F4/80-FITC | F4/80 | In house | FACS |
| Fibronectin (human/mouse) | rabbit | Sigma | IF |
| GFP | rabbit | Invitrogen | IF |

| | | | |
|---|---|---|---|
| Gr-1 | RB6-8C5 | In house | FACS |
| IgM | RMM-1 | Biolegend | FACS |
| IgG1, IgG2a, IgG2b, IgG3 or IgM (mouse) | goat | Southern Biotech | FACS |
| Laminin (human/mouse) | rabbit | Sigma | IF |
| LTβR | 3C8 | eBioscience | IF |
| LYVE1 | rabbit | ReliaTech | IF |
| MAdCAM-1-biotin | MECA-367 | eBioscience | FACS |
| MAdCAM-1 | MECA-89 | In house | IF |
| MHCII | M5/114.1 5.2 | In house, Biolegend | FACS |
| MHCII I-$A^P$ | 7-16.32 | Cedarlane | IF |
| PDGFRα | APA5 | Biolegend | IF |
| Pdpn | 8.1.1 | In house | FACS, IF |
| TCRβ | H57-597 | In house | FACS, IF |
| | | | |
| | | | |
| **Primary antibodies for human tissues** | **Clone or source** | **Supplier** | **Note** |
| BP3/CD157 | SY11B5 | eBioscience | IF |
| CD11c | BU83 | In house | IF |
| CD138 | B-A38 | AbD Serotec | IF |
| CD21 | HB5 | Thomas Tedder (Duke University) | IF |
| CD3 | OKT3 | In house | IF |
| CD31 | HEC7 | Thermo Scientific | IF |
| Lysosome | rabbit | Dako | IF |
| LYVE1 | 8C | David Jackson (Oxford univ.) | IF |
| Pdpn | D2-40 | Signet | IF |
| | | | |
| **Secondary antibodies to** | **Source** | **Supplier** | **Note** |
| goat IgG, Alexa Fluor 488 | donkey | Invitrogen | FACS, IF |
| goat IgG, Alexa Fluor 647 | donkey | Invitrogen | FACS, IF |
| rabbit IgG, Alexa Fluor 647 | donkey | Invitrogen | FACS, IF |
| rabbit IgG, Alexa Fluor 488 | donkey | Invitrogen | FACS, IF |
| rat IgG, Cy3 | donkey | Jackson Immunoresearch | IF |
| armenian hamster IgG biotin | goat | Jackson Immunoresearch | IF |

| | | | |
|---|---|---|---|
| syrian hamster IgG, horseradish peroxidase (HRP) | goat | Jackson Immunoresearch | IF |
| streptavidin HRP | - | Jackson Immunoresearch | IF |
| streptavidin-Cy3 | - | Jackson Immunoresearch | IF |
| Tyramide Alexa Fluor 488, Cy3 or Alexa Fluor 647 (using borate buffer) | - | Invitrogen | IF |

Additional antibodies used are listed in Link et al. (2).

**Table S2. qRT-PCR primer sequences.**

| Gene | Forward | Reverse |
|---|---|---|
| *April* | GGTGGTATCTCGGGAA GGAC | CCCCTTGATGTAAATGAAA GACA |
| *Baff* | AGACGCGCTTTCCAGG GACC | TAGTCGGCGTGTCGCTGTC TG |
| *Collagen1α1* | GCTCCTCTTAGGGGCC ACT | CCACGTCTCACCATTGGGG |
| *Collagen1α2* | GTAACTTCGTGCCTAGC AACA | CCTTTGTCAGAATACTGAG CAGC |
| *Cxcl12* | TGCATCAGTGACGGTA AACCA | TTCTTCAGCCGTGCAACAA TC |
| *Cxcl13* | GAGGCTCAGCACAGCA AC | TTGAAATCACTCCAGAACA CCTAC A |
| *Il6* | ATGGATGCTACCAAAC TGGAT | TGAAGGACTCTGGCTTTGT CT |

Additional primers used can be found in Link et al. (2).

## Supplementary Movies

**Movie S1. T zones and medulla exhibit marked differences of extracellular matrix structures.** 3D reconstruction of FRC and fibrillar collagen organization in LN. 2-photon image reconstruction of z stack (1 µm spacing) showing FRC (green) and fibrillar collagen as assessed by SHG (red) within a naive LN from a pCol-GFP mouse after volume rendering.

**Movie S2. PC/PB tightly interact with FRC in medullary cords.** 3D reconstruction of confocal images of vibratome sections (25 µm) from draining pLN of OVA/Mont immunized mice (with OT-I/II cell transfer, d5.5) stained for laminin (blue), $pdpn^+$ FRC (red) and $CD138^+$ PB/PC (green) with white areas representing contact zones between these two cell types within medullary cords.

**Movie S3. Migratory behavior of PC/PB in LN slices from immunized pCol-GFP mouse.** A LN slice stained with anti-CD138 antibodies (red) was imaged during 20 min with a confocal microscope in the outer T zone and the medullary cords. Frame intervals, 20 sec. The animation represents a single optical section of 10 µm taken 20 µm below the cut surface of the slice.

**Movie S4. PC/PB actively migrate in the outer T zone and thereby show transient interactions with multiple FRC**. LN slice from an immunized (SRBC, d6) pCol-GFP mouse was stained with anti-CD138 antibodies (red) and imaged during 20 min with a confocal microscope. The trajectory of the CD138-positive cells is represented in white. Frame intervals, 20 sec. The animation represents a single optical section of 10 µm taken 20 µm below the cut surface of the slice.

**Movie S5. PC/PB exhibit low motility and long-term interactions with single FRC within medullary cords**. A LN slice from immunized (SRBC, d6) pCol-GFP mouse was stained with anti-CD138 antibodies (red) and imaged during 20 min with a confocal microscope. Frame intervals, 20 sec. The animation represents a single optical section of 10 µm taken 20 µm below the cut surface of the slice.

**Movie S6. Medullary FRC exhibit marked shape changes as compared to TRC.** A LN slice from a pCol-GFP immunized (SRBC, day 7) mouse was imaged during 6 min with a confocal microscope in the outer T zone (left animation) or in a medullary cord (right animation). Frame intervals, 20 sec. The animations represent a single optical section of 10 µm taken 20 µm below the cut surface of the slice.

**Movie S7. Neutralizing antibodies to IL-6 do not alter the distribution nor the migration of CD138 positive cells in LN slices from immunized pCol-GFP mouse.** A LN slice from a pCol-GFP immunized (SRBC, day 7) mouse which had received anti-IL-6 antibodies at d2 and d5, was stained with anti-CD138 antibodies (red) and imaged during 20 min using a confocal microscope. Frame intervals, 20 sec. The animation represents a single optical section of 10 µm taken 20 µm below the cut surface of the slice.

## References


1. Asperti-Boursin, F., Real, E., Bismuth, G., Trautmann, A., and Donnadieu, E. (2007). CCR7 ligands control basal T cell motility within lymph node slices in a phosphoinositide 3-kinase-independent manner. *J Exp Med* 204, 1167-1179.
2. Link A, et al.(2007) Fibroblastic reticular cells in lymph nodes regulate the homeostasis of naive T cells. *Nat Immunol* 8(11):1255-1265.